Hindawi
Shock and Vibration
Volume 2023, Article ID 5597286, 12 pages
https://doi.org/10.1155/2023/5597286

Research Article

The Chaotic Property of BTA Deep-Hole Machining System under the Effect of Inner Cutting Fluid

Quanbin Zhang,[1] **Wu Zhao**,[1] **Yamin Li**,[1,2] **and Shuangxi Jing**[1]

[1]*School of Mechanical and Power Engineering, Henan Polytechnic University, Jiaozuo 454000, China*
[2]*College of Mechanical and Electrical Engineering, Xinxiang University, Xinxiang 453003, China*

Correspondence should be addressed to Wu Zhao; zhaowu@hpu.edu.cn

Received 9 April 2023; Revised 12 May 2023; Accepted 25 May 2023; Published 6 June 2023

Academic Editor: Francisco Beltran-Carbajal

To clarify the action mechanism of parameter change on system stability, the chaotic property of BTA deep-hole machining system under the effect of inner cutting fluid was analyzed. According to the kinematic characteristics of the internal cutting fluid and the equation of the moment of momentum of the system, the kinematic equation of the boring bar considering the effect of the internal fluid was established. The critical conditions of chaos were deduced according to the Hamiltonian function and Melnikov function of the plane near-Hamilton system. The mechanism of the liquid filling ratio, cutting fluid flow velocity, and frequency ratio parameters on the system's critical instability surface is investigated. The correlation and sensitivity of influencing factors, such as filling ratio and frequency ratio, and cutting fluid flow velocity to the sensitivity of system chaos are explored. The results show that in precision machining, the change of liquid filling ratio is positively related to the stability of the system, the change of cutting fluid flow velocity is negatively correlated with the stability of the system, and the change of frequency ratio has no monotonicity effect on the stability of the system. The sensitivity of the chaotic characteristics of the system to each parameter is bounded by the filling liquid ratio $h = 0.58$. When $0 \le h \le 0.58$, frequency ratio $\overline{\omega}$ > filling ratio h > cutting fluid flow velocity V_0; when $0.58 < h \le 1$, filling ratio h > frequency ratio $\overline{\omega}$ > cutting fluid flow velocity V_0. These research conclusions can lay a certain theoretical foundation for the analysis, control, and optimization of the complex mechanical behavior of BTA deep-hole machining systems in engineering practice.

1. Introduction

With the development of science and technology, mankind needs to face the constant challenges of aerospace, deep-sea, deep-earth, and other extreme environments; at the same time, in these extreme environments, there are many parts of scientific exploration equipment which are also facing the challenge of a high, precision, sharp limit bottleneck. The nonlinear characteristics of these high-precision parts during service have become a major factor affecting the overall dynamic stability of extreme equipment [1–3], among which the impact and application of high-precision deep-hole components with the large length-diameter ratio is particularly prominent in the abovementioned fields [4–7].

The Boring Trepanning Association (BTA) deep-hole machining can be classified into three categories: BTA system drilling, BTA trepanning drilling, and BTA boring. Among them, the former two are commonly used for processing solid components with low machining accuracy that require secondary precision machining, while the latter is often employed to expand holes in components with high machining accuracy and capability of achieving precision machining [8]. BTA deep-hole processing technology is an important means of processing deep-hole parts. Its system is a typical complex nonlinear process system that involves the coexistence and interaction of mechanical, electrical, and hydraulic fields. The complexity of its motion state lies in the simultaneous rotation and axial feed of the boring bar, accompanied by the inflow and outflow of cutting fluid. The

analysis of the chaotic characteristics of the system is crucial in elucidating the impact of parameter changes on system stability, which is essential for overcoming the quality bottleneck in deep-hole parts processing [9–12]. At present, there is no general analytical paradigm for analyzing a complex nonlinear dynamic system [13–16], which also brings great challenges to the dynamic stability analysis of complex BTA deep-hole machining system with mechanical, electrical, and hydraulic multifield coupling.

Chin et al. [17–19] studied transverse vibration frequency characteristics of BTA deep-hole boring bar under internal cutting fluid and axial pressure using the Euler–Bernoulli beam and Timoshenko beam as models, respectively. It is found that the natural frequencies of the same order modes under the two models are quite different, and the difference becomes more and more obvious with the change in boring bar speed. At the same time, the change of external force can also change the natural frequency of the system. Matsuzaki et al. [20, 21], on the premise of ignoring the influence of torsional vibration, axial force, and cutting fluid, established the motion equation of the bending boring bar and found that the natural frequency and natural mode of the boring bar will change complicated with the length of boring bar entering the workpiece. This means that when the bending vibration frequency of the boring bar is close to or lower than the natural frequency of the system, there will be rifling marks. To suppress the vibration of the system, Raabe et al. [22, 23] studied the flutter disturbance and spiral regeneration effect in the deep-hole machining system and simulated the correlation between the stability and instability of the system on the flutter and spiral through modeling. On this basis, Messaoud et al. [24–26] further proposed an online flutter monitoring strategy based on control chart through dynamic modeling of the nonlinear time series of the deep-hole machining system, and investigated the influence of the position of the adjusted guide block and drilling depth on the system chatter. Steininger and Bleicher [27] adopted a continuous multidimensional sensor system to monitor the dynamic disturbance of different parameter changes on the deep-hole machining system, and adjusted the parameter changes to deal with the system flutter and rotary vibration, which proved that variable speed cutting plays a role in improving the system stability.

The actual production system for BTA deep hole machining involves the rotation of the boring bar, which is accompanied by the inflow and outflow of cutting fluid. This creates a typical fluid-structure coupling system with multi-energy field nonlinear action between the boring bar and fluid. This further increases the complexity of the system analysis. Hu and Miao [28] derived the nonlinear expression of the cutting fluid reaction force acting on the rotating boring bar, established the basic motion equation of the rotating boring bar under the fluid-structure coupling, and obtained the basic criterion of the half-frequency vortices and instability of the boring bar caused by the cutting fluid, which laid a foundation for the subsequent in-depth analysis of the nonlinear characteristics of the fluid-structure coupling system in BTA deep-hole machining. In the nonlinear study of the fluid-structure coupling system, Utsumi [29] studied the nonlinear vibration characteristics of the simply supported cylindrical rotor under the fluid-structure coupling effect by the semianalytical method. The results show that increasing the fluid volume will reduce the excitation effect of nonlinear pressure gradient on the fluid velocity, and make the stability of the whole system stronger. Wang et al. [30, 31] analyzed the stability of a flexible rotor based on a Bernoulli–Euler beam. It is found that the unstable region of the system will gradually move to the low-speed region with the increase of the ratio of fluid mass to rotor mass. Firouz-Abadi et al. [32–34] applied the first-order shear deformation shell theory and quasi-dimensional linear Navier–Stokes theory to analyze the stability of rotating cylindrical shells under fluid-structure coupling and found that the stability of the system increases with the increase in the ratio of fluid mass to rotor mass. Zhao et al. [5, 35–37] combined the rod beam theory and the fluid-structure coupling theory and applied the system dynamics analysis method to establish the lateral nonlinear vibration model of the deep-hole boring bar containing the cutting fluid disturbance; analyzed the influence of the cutting fluid free surface, dynamic viscosity, system damping ratio and system cubic stiffness, and other parameters on the system vibration characteristics; and clarified the mechanism of the cutting fluid disturbance on the nonlinear vibration of the BTA deep-hole machining system. At the same time, the research on the external cutting fluid in the process of BTA deep-hole machining can be compared to the fluid motion between the slender ring gaps in the liquid-filled state, which has been thoroughly studied in fluid dynamics. While the inner cutting fluid is the fluid movement in the slender cylindrical cavity with an incomplete filling, its fluid state is complex [38–42] and its influence mechanism on the stability of the BTA deep-hole machining system is not clear. Therefore, it is necessary to further study the mechanism of the fluid-structure coupling effect formed by the internal cutting fluid on the BTA deep-hole machining system.

To explore the chaotic property of the BTA deep-hole machining system under the fluid effect of internal cutting fluid, this paper firstly established the system's equation of motion by considering the dynamic characteristics of the system under the fluid effect of the internal cutting fluid, and then based on the Hamiltonian function and Melnikov function under the near-Hamilton plane system, the critical conditions for the chaos of the system are deduced. Secondly, digital simulation was used to study the mechanism of the effect of the liquid filling ratio of the internal cutting fluid, the flow rate of the internal cutting fluid, and the frequency ratio on the critical unstable surface of the system in the processing system is studied. Finally, through the change of the filling ratio and the frequency ratio, the joint action relationship between the torque coefficient and the resultant force of the fluid force and the cutting force is explored, and the theoretical analysis conclusion is checked and verified with the physical experimental results.

2. Chaos of Lateral Vibration in BTA Deep-Hole System under the Effect of Inner Cutting Fluid

To describe the motion state of the boring bar, the coordinate system of the BTA deep-hole machining system, as shown in Figure 1, is established according to the actual working conditions of the BTA deep-hole machining system under the consideration of the fluid effect of internal cutting fluid.

In Figure 1, o-xyz is the coordinate system of the boring bar body, o-$x_a y_a z_a$ is the boring bar axis coordinate system, o-$x_c y_c z_c$ is the coordinate system of boring bar velocity, o-$\xi\eta\zeta$ is the rotating coordinate system of the boring bar, α is the nutation angle, β is the precession angle, γ is the angle of rotation, u and v are the radial and tangential disturbance velocities of fluid in the cylindrical coordinate system, respectively, r and θ are polar coordinates in the cylindrical coordinate system, o' is the axis of the boring bar under ideal condition, Ω is the speed at which the boring bar rotates around its axis of symmetry (z_c) in the velocity coordinate system (o-$x_c y_c z_c$), F_{xa} and F_{ya} are the components of the combined force of fluid force and cutting force in the direction of x_a and y_a, respectively, and P_1 is the total axial pressure ($P_1 = P_{xa} + P_{ya}$, P_{xa}, and P_{ya} are the components of the additional axial force of boring bar in the direction of x_a and y_a, respectively).

2.1. Motion Equation of BTA Deep-Hole Machining System under Internal Cutting Fluid Effect. When only considering the fluid effect of the internal cutting fluid, the motion state of the cutting fluid at any position in the flow field can be represented by polar coordinates (as shown in Figure 1), and the relative disturbance velocity of the cutting fluid ($\vec{v}_r$) can be expressed as follows:

$$\vec{v}_r = \mathrm{u}\vec{\mathrm{r}} + v\vec{\theta}. \tag{1}$$

Thus, the linearized motion equation and continuity equation of ideal incompressible fluid can be obtained as follows:

$$\frac{\partial \vec{v}_r}{\partial t} + 2\vec{\omega}_2 \times \vec{v}_r = -\frac{\nabla P_2}{\rho_f} - \vec{a}_e, \tag{2}$$

$$\mathrm{div}\,\vec{v}_r = 0, \tag{3}$$

where $P_2 = P_3 - \rho_f \omega_2^2 (r^2 - b^2)/2$ is the radial disturbance pressure field, ρ_f is the cutting fluid density, P_3 is the radial fluid pressure of the cutting fluid, which is a function of (r, θ), ω_2 is the disturbance frequency of cutting fluid, b is the radius of the free liquid surface, and $\vec{a}_e$ is the implicated acceleration at any point.

Substitute equations (3) into (2) and take div to get

$$\Delta P_2 = 0, \tag{4}$$

where Δ is the Laplace operator.

The boundary conditions of the flow field are determined as follows:

$$u|_{r=d_1/2} = 0, \tag{5}$$

where d_1 is the inner diameter of the boring bar.

In the BTA deep-hole processing system, $r = b + \tau(\theta, t)$, where τ is a first-order small quantity and the radial disturbance velocity on the free surface is $u|_{r=b} = \partial\tau/\partial t$. Considering that the relative pressure on the free surface in the boring bar is zero, the radial disturbed pressure field is $P_2|_{r=b} = -\rho_f \omega_2^2 b\tau$, and the boundary conditions on the free surface can be finally determined as follows:

$$\left.\frac{\partial P_2}{\partial t}\right|_{r=b} = -\rho_f \omega_2^2 \mathrm{bu}|_{r=b}. \tag{6}$$

Assuming that the x_a, y_a, and z axes coincide with the central inertia axis of the system to the center of mass, K is the polar moment of inertia, N is the lateral moment of inertia, and the moment of momentum of the system can be expressed as follows:

$$Q = \begin{bmatrix} K\omega_{xa} + Q_{2xa} & N\omega_{ya} + Q_{2ya} & N\omega_z + Q_{2z} \end{bmatrix}^T, \tag{7}$$

where $\omega_{\mathrm{xa}} = -\dot{\beta}\sin\alpha$, $\omega_{\mathrm{ya}} = \dot{\alpha}$, $\omega_z = \dot{\gamma} + \omega_{\mathrm{za}}$, and $\omega_{\mathrm{za}} = \dot{\beta}\cos\alpha$. The projections of the relative disturbance velocity v_r of the cutting fluid on the x_a, y_a, and z axes are v_{r1}, v_{r2}, and v_{r3}, respectively; $Q_{2\mathrm{xa}}$, $Q_{2\mathrm{ya}}$, and Q_{2z} are, respectively, represented as follows:

$$\begin{aligned}
Q_{2xa} &= \rho_f \int_\tau \left[\left(z^2 + y_A^2\right)\omega_{\mathrm{xa}} - z x_a \omega_x + y_a v_{r3} - x_a y_a \omega_{\mathrm{ya}} - z_a v_{r3} \right] \mathrm{d}t, \\
Q_{2ya} &= \rho_f \int_\tau \left[\left(z^2 + x_a^2\right)\omega_{\mathrm{xa}} + z v_{r1} - z y_a \omega_z - x_a y_a \omega_{\mathrm{xa}} - x_a v_{r3} \right] \mathrm{d}t, \\
Q_{2z} &= \rho_f \int_\tau \left[\left(x_a^2 + y_a^2\right)\omega_z + x_a v_{r2} - z x_a \omega_{\mathrm{xa}} - z y_a \omega_{\mathrm{ya}} - y_a v_{r1} \right] \mathrm{d}t.
\end{aligned} \tag{8}$$

Then, the components M_{xa}, M_{ya}, and M_z of the momentum moment equation on the x_a, y_a, and z axes are follows:

$$\left.\begin{aligned} M_{\mathrm{xa}} &= N\dot{\omega}_{\mathrm{xa}} + K\omega_z\omega_{\mathrm{ya}} - N\omega_{\mathrm{ya}}\omega_{\mathrm{za}} + \dot{Q}_{2xa} + Q_{2z}\omega_{\mathrm{ya}} - Q_{2\mathrm{ya}}\omega_{\mathrm{za}} \\ M_{\mathrm{ya}} &= N\dot{\omega}_{\mathrm{ya}} + N\omega_z\omega_{\mathrm{xa}} - K\omega_{\mathrm{xa}}\omega_{\mathrm{za}} + \dot{Q}_{2ya} + Q_{2xa}\omega_{\mathrm{za}} - Q_{2z}\omega_{\mathrm{xa}} \\ M_z &= K\dot{\omega}_z + Q_{2z} + \dot{Q}_{2\mathrm{ya}}\omega_{\mathrm{xa}} - Q_{2xa}\omega_{ya} \end{aligned}\right\}. \tag{9}$$

Equation (9) is the global motion model of the BTA deep-hole machining system considering various factors in the working process. The analysis of this equation needs to be combined with equations (2) and (3), taking into account the boundary conditions of cutting fluid motion, that is, equations (5) and (6).

In actual production processes, precision deep hole processing typically employs a post-guidance mode in technology. This involves installing the guide key behind the tool with the feed direction of the tool as its front. When considering the fluid effect, $M_{xa} = M_{ya} = M_z = 0$. It is also assumed that the viscosity of cutting fluid $\mu = 0$. In the generalized coordinates α, β, γ, x_a, y_a, and z, the kinetic energy of the system can be written as follows:

$$\begin{aligned} T &= \frac{1}{2}\left[K\omega_z^2 + N\omega_{xa}^2 + N\omega_{\mathrm{ya}}^2 + Q_{2z}\omega_z + Q_{2\mathrm{xa}}\omega_{\mathrm{xa}} + Q_{2\mathrm{ya}}\omega_{\mathrm{ya}}\right] + \frac{\rho_f}{2}\int_\tau \left(v_{r1}^2 + v_{r2}^2 + v_{r3}^2\right)\mathrm{d}\tau \\ &= \frac{1}{2}\left[K(\dot{\gamma} + \dot{\beta}\cos\alpha)^2 + N\left(\dot{\beta}^2\sin^2\alpha + \dot{\alpha}^2\right) + Q_{2z}(\dot{\gamma} + \dot{\beta}\cos\alpha) - Q_{2\mathrm{xa}}\dot{\beta}\sin\alpha + Q_{2\mathrm{ya}}\dot{\alpha}\right] \\ &\quad + \frac{\rho_f}{2}\int_\tau \left(v_{r1}^2 + v_{r2}^2 + v_{r3}^2\right)\mathrm{d}\tau. \end{aligned} \tag{10}$$

According to the Lagrange principle, β and γ are cyclic coordinates. After cyclic integration, we can get

$$\begin{cases} K(\dot{\gamma} + \dot{\beta}\cos\alpha) + Q_{2z} = \varphi_\gamma, \\ K(\dot{\gamma} + \dot{\beta}\cos\alpha)\cos\alpha + N\dot{\beta}\sin^2\alpha + Q_{2z}\cos\alpha - Q_{2xa}\sin\alpha = \varphi_\beta. \end{cases} \tag{11}$$

The reaction torque of the internal cutting fluid on the system is as follows:

$$\begin{aligned} M_{\mathrm{Lxa}} + iM_{\mathrm{Lya}} &= m_f d_1^2 \gamma\omega_2 \left[F_{\mathrm{LSM}} + iF_{\mathrm{LIM}}\right] e^{i\omega_2 t}\sin^2\alpha, \\ M_{\mathrm{Lya}} &= m_f d_1^2 \gamma\omega_2 \sin\alpha\left[F_{\mathrm{LSM}}\sin\omega_2 t + F_{\mathrm{LIM}}\cos\omega_2 t\right], \\ M_{\mathrm{Lz}} &= m_f d_1^2 \dot{\gamma}\omega_2 F_{\mathrm{LRM}}\sin^2\alpha e^{i2\Omega t}, \end{aligned} \tag{12}$$

where m_f is the mass of cutting fluid, $F_{\mathrm{LRM}} = -F_{\mathrm{LSM}}$ is the gyro torque coefficient, and F_{LIM} is the phase plane torque coefficient. All these can be expressed as functional relations related to the vibration frequency of cutting fluid, boring bar size, liquid filling ratio, viscosity coefficient of cutting fluid, and other parameters, which can reflect the relationship between the fluid characteristics of internal cutting fluid and torque coefficient in the internal structure of the boring bar.

Under the general working condition, the damping moment generated by considering the deviation of boring bar axis is as follows:

$$M_y = \mathrm{NV}_0^2 k_y \sin\alpha - \mathrm{NV}_0 k_{\mathrm{yy}}\dot{\alpha}, \tag{13}$$

where k_y is the characteristic number of the static moment, k_{yy} is the characteristic number of damping torque, and V_0 is the flow velocity of the inner cutting fluid.

Combined equation (11) can be deduced as follows:

$$\varphi_\gamma - Q_{2z} = \varphi_{\gamma L}, \varphi_\gamma - Q_{2z}\cos\alpha + Q_{2xa}\sin\alpha = \varphi_{\beta L}. \tag{14}$$

Substituting it into f equations (11), (12), and (9), we get the motion equation of the boring bar deflection angle (α) as follows:

$$N\ddot{\alpha} + \frac{\varphi_{\gamma L}\left(\varphi_{\beta L} - \varphi_{\gamma L}\cos\alpha\right)}{N\sin\alpha} - \frac{\left(\varphi_{\beta L} - \varphi_{\gamma L}\cos\alpha\right)^2\cos\alpha}{N\sin^3\alpha} = NV_0^2 k_y\sin\alpha - NV_0 k_{\mathrm{yy}}\dot{\alpha} + M_{\mathrm{Lya}}. \tag{15}$$

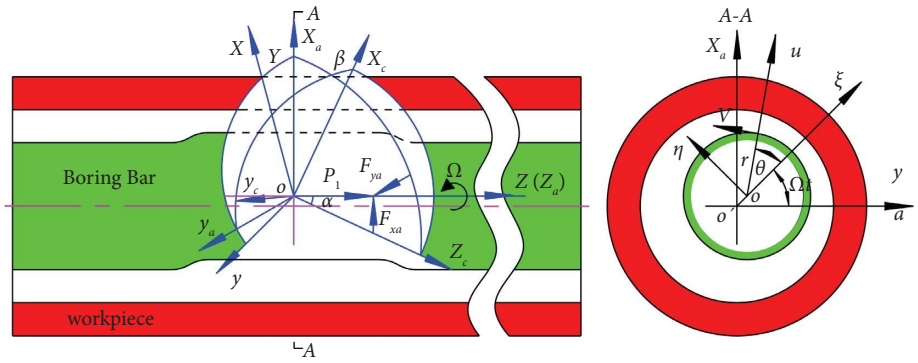

Figure 1: Coordinate system of BTA deep-hole machining system.

2.2. Critical Conditions of Chaos in BTA Deep-Hole Machining System under the Internal Cutting Fluid Effect. The strong nonlinear term in equation (15) near zero point exists as follows:

$$\varphi_\gamma = \varphi_\beta = K\dot{\gamma}, Q_{2z} = K_L\dot{\gamma}, Q_{2xa} = Q_{2ya} = 0. \tag{16}$$

Performing a Taylor expansion on equation (15), and utilizing the approximation $\sin\alpha = \alpha - \alpha^3/6 + o(\alpha)^5$, equation (15) can be simplified to:

$$\ddot{\alpha} + D_f\dot{\alpha}/V_0 + \left[\eta\omega_0^2 - \frac{\sigma_p F\sin(\omega_2 t + \upsilon_0)}{V_0}\right]\alpha - \left[\phi\omega_0^2 - \frac{\sigma_p F\sin(\omega_2 t + \upsilon_0)}{(6V_0)}\right]\alpha^3 = 0, \tag{17}$$

where

$$\begin{aligned}
\eta\omega_0^2 &= \left(\frac{\varphi_\gamma^2}{4N^2} - \frac{\varphi_\gamma K_L\gamma}{2N^2} - V_0^2 k_y\right),\\
\phi\omega_0^2 &= \frac{1}{6}\left(\frac{43\varphi_\gamma^2}{4N^2} + \frac{\varphi_\gamma K_L\gamma}{4N^2} - V_0^2 k_y\right),\\
D_f &= V_0^2 k_{yy},\\
\sigma_p &= \frac{m_f d_1^2\gamma\omega_2 V_0}{(4N)},\\
F &= \sqrt{F_{\mathrm{LSM}}^2 + F_{\mathrm{LIM}}^2},\\
\upsilon_0 &= \tan^{-1}\left(\frac{F_{\mathrm{LIM}}}{F_{\mathrm{LIM}}}\right),\\
K_L &= \pi\rho_f L\frac{d_1^4}{32},\\
N &= \frac{\pi\rho_s L}{192}\left[3\left(d_2^4 - d_1^4\right) + 4L^2\left(d_2^2 - d_1^2\right)\right],\\
\varphi_\gamma &= \pi\rho_s L\dot{\gamma}\frac{\left(d_2^4 - d_1^4\right)}{32},\\
m_f &= \frac{d_1^2}{4}\pi\left(1 - h^2\right)L\rho_f,
\end{aligned} \tag{18}$$

where K_L is the polar moment of inertia of the internal cutting fluid.

According to the universality condition of the system operation, there exists $\varepsilon = 1/V_0 \ll 1$, and by substituting $z_1 = \alpha$, $z_2 = \dot{\alpha}$, and $v = \omega_2 t + v_0$ as follows, equation (17) can be transformed into

$$\left.\begin{aligned} \dot{z}_1 &= z_2 \\ \dot{z}_2 &= -\eta\omega_0^2 + \phi\omega_0^2 z_1^3 + \varepsilon\left[\sigma_p F \sin v\left(z_1 - z_1^3/6\right) - D_f z_2\right] \\ \dot{v} &= \omega_2 \end{aligned}\right\}. \tag{19}$$

Determining $\varepsilon = 0$, there is a Hamiltonian function for (z_1, z_2) components:

$$H = \frac{z_2^2}{2} + \frac{\eta\omega_0^2}{2} z_1^2 - \frac{\varphi\omega_0^2}{4} z_1^4. \tag{20}$$

Thus, equation (20) has hyperbolic periodic orbits in z_1-z_2-v phase space:

$$X = \left[\overline{z}_1, \overline{z}_2, v(t)\right] = \left(\sqrt{\eta/\phi}, 0, \omega_2 t + v_0\right) = \left(-\sqrt{\eta/\phi}, 0, \omega_2 t + v_0\right), \tag{21}$$

and connected by a pair of the heteroclinic orbits:

$$\left[\overline{z}_{1h}^{\pm}(t), \overline{z}_{2h}^{\pm}(t), v(t)\right] = \left[\pm\sqrt{\frac{\eta}{\phi}}\tanh\left(\sqrt{\frac{\eta}{2}}\omega_0 t\right), \pm\frac{\eta\omega_0}{2}\sqrt{\frac{2}{\phi}}\operatorname{sech}^2\left(\sqrt{\frac{\eta}{2}}\omega_0 t\right), \omega_2 t + v_0\right], \tag{22}$$

when $z_2 > 0$, "+" is taken in equation (22); when $z_2 < 0$, "−" is taken in equation (22); and the components of (z_1, z_2) can be obtained by the plane curve of $H = \eta^2\omega_0^2/(4\phi)$.

When $\varepsilon \neq 0$, the hyperbolic periodic orbit also exists in equation (19), denoted as X_ε, in which the stable manifold is denoted as $R^s(X_\varepsilon)$, and the unstable manifold is denoted as $R^u(X_\varepsilon)$. By the Melnikov function method, we can get

$$\begin{aligned} &X^{\pm}\left(t_0, v_0, \sigma_p, F, D_f, \omega_2\right) \\ &= \int_{-\infty}^{\infty} x_{2h}^{\pm}(t)\left\{\sigma_p F\left[x_{1h}^{\pm}(t) - \frac{1}{6}x_{1h}^{\pm 3}(t)\sin\left[\omega_2(t + t_0) + v_0\right] - D_f x_{2h}^{\pm}(t)\right]\right\}\mathrm{d}t \\ &= \frac{\sigma_p F\pi\omega_2^2}{\varphi\omega_0^2}\operatorname{csch}\left(\frac{\pi\omega_2}{\omega_0\sqrt{2\eta}}\right)\cos\left(\omega_2 t_0 + v_0\right) - \frac{2D_f\eta\sqrt{2\eta}\omega_0}{3\phi} \\ &\quad - \frac{\sigma_p F\eta\pi\omega_2^2}{9\varphi^2\omega_0^2}\left(1 - \frac{3\omega_2^2}{4\eta\omega_0^2}\right)\operatorname{csch}\left(\frac{\pi\omega_2}{\omega_0\sqrt{2\eta}}\right)\cos\left(\omega_2 t_0 + v_0\right). \end{aligned} \tag{23}$$

The condition for the intersection of $R^s(X_\varepsilon)$ and $R^u(X_\varepsilon)$ is as follows:

$$R^0(\omega_2) = \frac{2\sqrt{2}\omega_0^3\eta^{(3/2)}\sinh\left(\pi\omega_2/\omega_0\sqrt{2\eta}\right)}{3\pi\omega_2^2\left[1 - \eta/(9\phi) + (\omega_2)/(12\omega_0\phi)\right]}. \tag{24}$$

From the intersection of stable and unstable manifolds of hyperbolic fixed points on the cross section [43], it can be seen that, when $\sigma_p F/D_f > R^0(\omega_2)$, two manifold cross sections intersect; when $\sigma_p F/D_f < R^0(\omega_2)$, the cross sections of the two manifolds never intersect; and when $\sigma_p F = D_f R^0(\omega_2)$, the quadratic heterologous bifurcation occurs.

So, the critical condition for chaos in BTA deep-hole machining system is $\sigma_p F/D_f < R^0(\omega_2)$. Substitute equations (18) and (24) into this critical condition to obtain

$$\frac{m_f d_1^2\dot{\gamma}\omega_2}{4NV_0 k_{yy}}\sqrt{F_{\mathrm{LSM}}^2 + F_{\mathrm{LIM}}^2} < \frac{2\sqrt{2}\omega_0^3\eta^{(3/2)}\sinh\left(\pi\omega_2/\omega_0\sqrt{2\eta}\right)}{3\pi\omega_2^2\left[1 - \eta/(9\phi) + (\omega_2)/(12\omega_0\phi)\right]}. \tag{25}$$

Let $h = 2b/d_1$ and $\overline{\omega} = \omega_2/\omega_0$, equation (54) can be converted into

$$\sqrt{F_{LSM}^2 + F_{\mathrm{LIM}}^2} < \frac{32\sqrt{2}\eta^{(3/2)} N V_0 k_{yy} \sin\mathrm{h}\left(\sqrt{2\eta}\,\pi\overline{\omega}\right)}{3\pi^2\overline{\omega}^3\left[1-\eta/(9\phi)+\overline{\omega}/(12\phi)\right]\left(1-h^2\right)L\rho_f d_1^4\dot{\gamma}}. \tag{26}$$

Let $f = (32\sqrt{2}\,\eta^{(3/2)} N V_0 k_{yy} \sin\mathrm{h}\ (\sqrt{2\eta}\,\pi\overline{\omega}))/(3\pi^2\overline{\omega}^3[1-\eta/(9\phi)+\overline{\omega}/(12\phi)](1-h^2)L\rho_f d_1^4\dot{\gamma})$, then the critical condition for chaos in the BTA deep-hole machining system is as follows:

$$\sqrt{F_{\mathrm{LSM}}^2 + F_{\mathrm{LIM}}^2} < f. \tag{27}$$

2.3. Chaotic Characteristics of the System with Parameter Changes. Combined with the actual BTA deep-hole machining system, the simulation parameters are selected as follows: $d_1 = 30\,\mathrm{mm}$ $D_1 = 46\,\mathrm{mm}$, $\rho_s = 7.87\times10^3\,\mathrm{kg/m^3}$, $\rho_f = 0.865\times10^3\,\mathrm{kg/m^3}$, $\dot{\gamma} = 25$, $k_{yy} = 10^{-3}$, $k_y = 0.05$, $0 \le h \le 1$, $0 \le \overline{\omega} \le 6$, and $0 \le V_0 \le 15\,\mathrm{m/s}$. Through the change of filling ratio h, frequency ratio $\overline{\omega}$, and cutting fluid flow velocity V_0, equation (27) is numerically simulated, and the chaotic characteristics of the system are analyzed. The numerical simulation is shown in Figures 2 and 3.

Under different cutting fluid flow velocities, the effects of the filling ratio and frequency ratio on the chaotic characteristics of the system are shown in Figures 2(a)–2(c). From Figure 2(a), it can be seen that with the increase of the liquid filling ratio h, the torque coefficient $\sqrt{F_{\mathrm{LSM}}^2 + F_{\mathrm{LIM}}^2}$ value represented by the curved surface f decreases continuously, which means that the area of chaos in the system becomes smaller. Figures 2(b) and 2(c) show the influence of cutting fluid flow velocity V_0 change on the chaotic characteristics of the system. The results show that the torque coefficient $\sqrt{F_{\mathrm{LSM}}^2 + F_{\mathrm{LIM}}^2}$ value represented by surface f increases with the increase of cutting fluid velocity V_0. This means that the region where chaos occurs gradually becomes larger and the instability of the system is intensified. Therefore, the increase of cutting fluid velocity in the boring bar will accelerate the transition process from laminar flow to turbulent flow, which makes the fluid disturbance enhance and aggravate the instability of the system.

The physical meaning of the positive and negative frequencies in the complex frequency is the frequency when the rotation factor is rotated counter clockwise, it is a positive frequency, and the frequency when it is rotated clockwise, it is a negative frequency. In Figure 2(a), the influence of frequency ratio $\overline{\omega}$ change on chaotic characteristics of the system is as follows: when the absolute value of frequency ratio $\overline{\omega}$ decreases monotonically within the interval $-6 \le \overline{\omega} \le -3$, the torque coefficient $\sqrt{F_{\mathrm{LSM}}^2 + F_{\mathrm{LIM}}^2}$ value represented by surface f decreases. This shows that the decrease of frequency ratio $\overline{\omega}$ in this range will promote the stability of the system. When the absolute value of frequency ratio $\overline{\omega}$ decreases monotonically within the interval $-3 < \overline{\omega} \le -1$, the torque coefficient $\sqrt{F_{\mathrm{LSM}}^2 + F_{\mathrm{LIM}}^2}$ value represented by the surface f increases, which means that the chaotic region of the system becomes larger. It shows that the decrease in the frequency ratio value in this region will intensify the instability and chaos of the system. When the frequency ratio $\overline{\omega}$ continues to decrease in the absolute value of interval $-1 < \overline{\omega} \le -0.6$, the value of the surface f decreases, that is to say, the chaotic region of the system becomes smaller. This indicates that the reduction of frequency ratio $\overline{\omega}$ in the interval will promote the stability of the system. In the interval $-0.6 < \overline{\omega} \le 0$, the surface f value increases with the decrease of the frequency ratio $\overline{\omega}$ value, which indicates that the chaotic region of the system becomes larger and the instability of the system is intensified. In the interval $0 < \overline{\omega} \le 1.4$, the value of the surface f decreases with the increase of the frequency ratio $\overline{\omega}$ value, which means that the chaotic region of the system becomes smaller. This indicates that the increase of frequency ratio $\overline{\omega}$ in the interval is beneficial to the stability of the system. In the interval $1.4 < \overline{\omega} \le 6$, the surface f value increases with the increase of frequency ratio $\overline{\omega}$, which indicates that the chaotic region of the system becomes larger and the instability of the system is intensified. Similarly, in Figures 2(b) and 2(c), the influence trend of frequency ratio $\overline{\omega}$ changes considering different cutting fluid flow velocities on chaotic characteristics of the system is consistent with the abovementioned law.

The effects of cutting fluid flow velocity and frequency ratio on the chaotic characteristics of the system under different filling ratios are shown in Figure 3. According to the comprehensive analysis of Figures 2 and 3, the following conclusions can be drawn from the physical mechanism. The increase of the liquid filling ratio reduces the chaotic characteristics of the system. The increase in cutting fluid velocity changes the fluid motion pattern, intensifies the chaotic characteristics of the system, and makes the stability of the system deteriorate. When the frequency ratio changes in the small value interval, it is not easy to trigger the frequency doubling relationship between the disturbance frequency and the system frequency, which reduces the probability of resonance of the system, so the stability of the system is better; when the frequency ratio changes in a large value range, the frequency doubling relationship between the disturbance frequency and the system frequency is easy to trigger, and the probability of resonance of the system increases, so the stability of the system is poor.

To further clarify the sensitivity of the chaotic characteristics of the system to the frequency ratio, the liquid filling ratio, and the cutting fluid flow velocity, a sensitivity analysis of equation (26) is carried out, as shown in Figure 4:

In Figure 4(a), to further clarify the boundary region, the expression of the critical curve can be obtained by data fitting the intersecting lines of two sensitive surfaces as follows: $f(V_0, h) = V_0 - 0.2631h^{-1.239}$. Furthermore, it can be seen that in Figure 4(a), when coordinate (V_0, h) makes function $f(V_0, h) > 0$, the sensitivity of chaotic characteristics of the system to liquid filling ratio h is greater than that of cutting fluid flow velocity V_0. When the coordinate (V_0, h) makes the function $f(V_0, h) \le 0$, the sensitivity of the chaotic characteristics of the system to the liquid filling ratio h is less

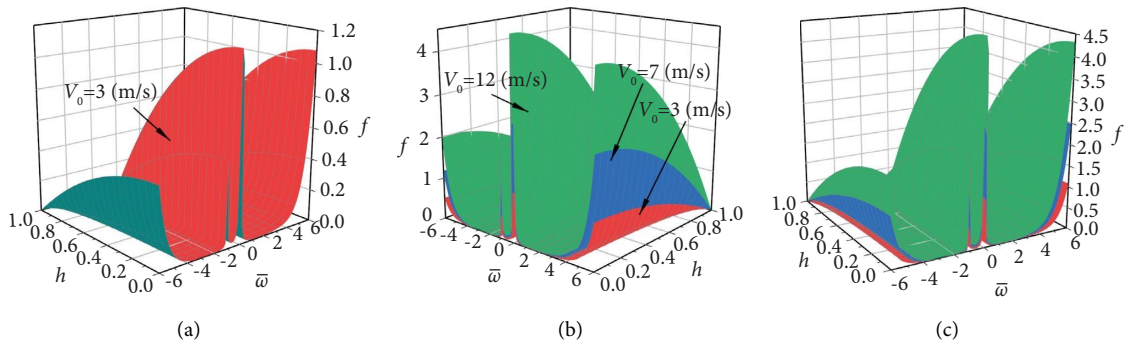

FIGURE 2: Influence of liquid filling ratio and frequency ratio on system chaotic characteristics under different cutting fluid flow velocities.

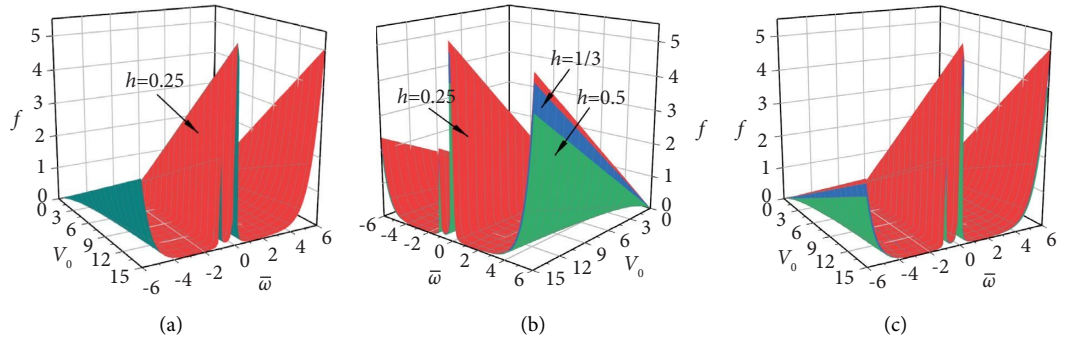

FIGURE 3: Effects of cutting fluid flow velocity and frequency ratio on chaotic characteristics of the system under different filling ratios.

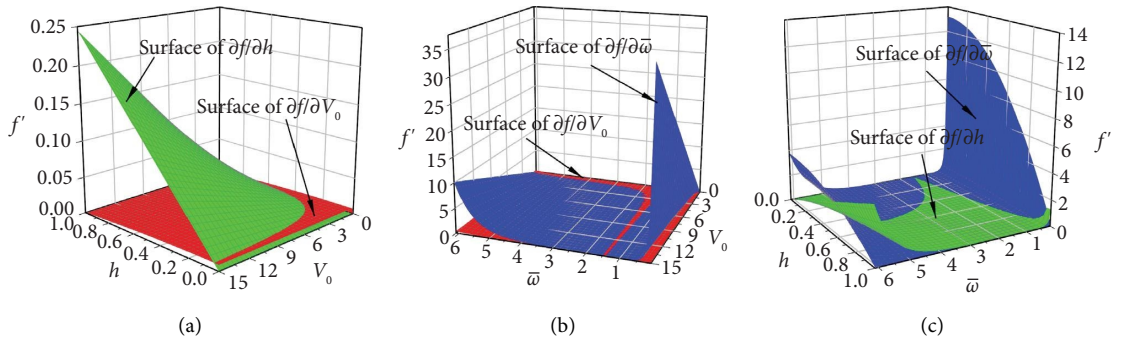

FIGURE 4: Sensitivity analysis of f to h, V_0, and $\overline{\omega}$: (a) $0 \le h \le 1$, $\overline{\omega} = 0.382$, sensitivity of f to h and V_0 when $0 \le V_0 \le 15$ m/s. (b) $h = 0.25$, $0 \le \overline{\omega} \le 6$, sensitivity of f to $\overline{\omega}$ and V_0 when $0 \le V_0 \le 15$ m/s. (c) $0 \le h \le 1$, $0 \le \overline{\omega} \le 6$, sensitivity of f to h and $\overline{\omega}$ when $V_0 = 5.2061$ m/s.

than or equal to the sensitivity of the cutting fluid flow velocity V_0.

In Figure 4(b), the sensitivity of the chaotic characteristics of the system to the frequency ratio $\overline{\omega}$ is greater than that of the cutting fluid flow velocity V_0 in most regions. Only in the frequency ratio $\overline{\omega}$ when the value is taken near 1.5 or the cutting fluid flow velocity V_0 is taken in the range of $0 \le V_0 \le 0.67$, the chaotic characteristics of the system are more sensitive to the frequency ratio $\overline{\omega}$ than to the velocity of cutting fluid V_0. To further clear the boundary area, the critical curve is obtained by data fitting expression as follows: when $0 < \overline{\omega} < 1.5$, $f(V_0, \overline{\omega}) = V_0 - 0.0586e^{3.8746\overline{\omega}}$; when $6 \ge \overline{\omega} \ge 1.5$, $f(V_0, \overline{\omega}) = V_0 - 14.92\overline{\omega}^{-2.286}$. Furthermore, it can be seen that in Figure 4(b), when coordinate $(V_0, \overline{\omega})$ makes function $f(V_0, \overline{\omega}) > 0$, the sensitivity of chaotic characteristics of the system to the frequency ratio $\overline{\omega}$ is greater than that of cutting fluid flow velocity V_0. When the coordinate $(V_0, \overline{\omega})$ makes the function $f(V_0, \overline{\omega}) \le 0$, the sensitivity of the chaotic characteristics of the system to the frequency ratio $\overline{\omega}$ is less than or equal to the sensitivity of the cutting fluid flow velocity V_0.

In Figure 4(c), the sensitivity of chaotic characteristics of the system to the frequency ratio $\overline{\omega}$ and cutting fluid flow velocity V_0 is bounded by the liquid filling ratio $h = 0.58$. When the liquid filling ratio $0 \le h \le 0.58$, the sensitivity of chaotic characteristics of the system to the frequency ratio $\overline{\omega}$

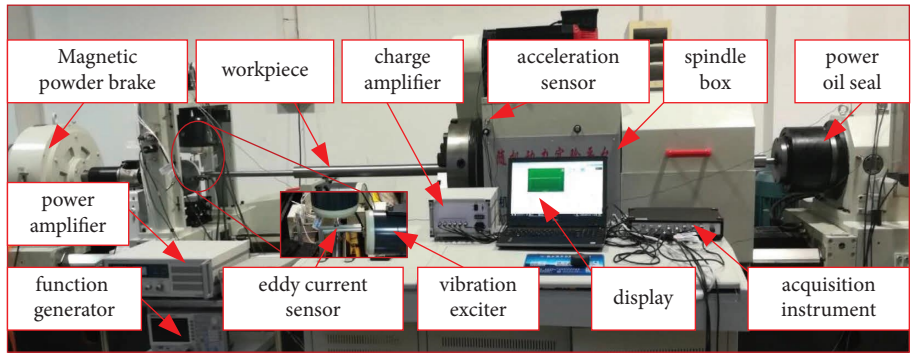

(a)

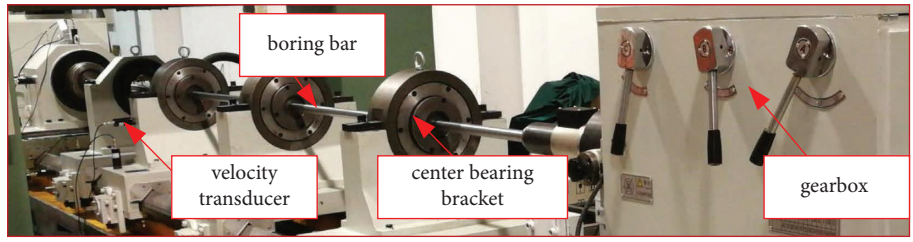

(b)

Figure 5: The experimental platform of BTA deep-hole processing: (a) the left half of the experimental platform and (b) the right half of the experimental platform.

is greater than that to the liquid filling ratio h in most areas. When the liquid filling ratio is $0.58 < h \le 1$, the sensitivity of chaotic characteristics to the frequency ratio $\overline{\omega}$ is less than that to the liquid filling ratio h in most regions. To further clear the boundary area, the critical curve is obtained by data fitting expression as follows: when $0 < \overline{\omega} < 1.5$, $f(h, \overline{\omega}) = h - 0.0399\overline{\omega}^2 + 0.3872\overline{\omega} - 0.3482$; when $6 \ge \overline{\omega} \ge 1.5$, $f(h, \overline{\omega}) = h + 0.209\overline{\omega}^2 + 0.4008\overline{\omega} - 0.9541$. When coordinate $(h, \overline{\omega})$ makes function $f(h, \overline{\omega}) > 0$, the sensitivity of chaotic characteristics of the system to the frequency ratio $\overline{\omega}$ is greater than that of the liquid filling ratio h. When the coordinate $(h, \overline{\omega})$ makes the function $f(h, \overline{\omega}) \le 0$, the sensitivity of the chaotic characteristics of the system to the frequency ratio $\overline{\omega}$ is less than or equal to the sensitivity of the liquid filling ratio h.

To sum up, in most regions, the sensitivity of the chaotic characteristics of the system to liquid filling ratio h is greater than that of cutting fluid flow velocity V_0, and the sensitivity of the chaotic characteristics of the system to the frequency ratio $\overline{\omega}$ is greater than the sensitivity to the cutting fluid flow velocity V_0, while the sensitivity of the chaotic characteristics of the system to the liquid-filled ratio V_0, and the frequency ratio $\overline{\omega}$ needs to be judged based on the position of the coordinate point in the function. Given a set of parameters, the sensitivity order of the chaotic characteristics of the system to the liquid filling ratio h, cutting fluid flow velocity V_0, and frequency ratio $\overline{\omega}$ can be quickly determined by the abovementioned method. From the perspective of qualitative analysis, it can be considered that in most of the value regions, the chaotic characteristics of the system are sensitive to frequency ratio, liquid filling ratio, and cutting fluid flow velocity in the following order: when $0 \le h \le 0.58$, the sensitivity of chaotic characteristics of the system to each parameter from strong to weak is frequency ratio $\overline{\omega}$, filling ratio h, and flow rate of cutting fluid V_0; when $0.58 < h \le 1$, the sensitivity of chaotic characteristics of the system to each parameter from strong to weak is filling ratio h, frequency ratio $\overline{\omega}$, and cutting fluid flow velocity V_0.

3. Experimental Demonstration

3.1. Experimental Equipment and Scheme. Select a boring bar made of 30CrMnSi and make a precision boring process for a deep hole with an inner diameter of ∅50 mm ($d_2 = \varnothing 50$ mm), in which the boring bar size is $D_1 = \varnothing 46$ mm, $d_1 = \varnothing 30$ mm, and $L = 9$ m. The workpiece material is 35CrNiMoV, where the elastic modulus $E = 214 \times 10^3$ MPa, shear modulus $G = 82.9 \times 10^3$ MPa, and Poisson's ratio $\mu = 0.3$. By changing the test condition, the influence of parameter change on the dynamic stability of the system is studied.

3.1.1. Experimental Equipment. The test equipment is composed of a deep-hole processing machine tool, power module, signal acquisition module, and signal analysis module. The test platform built is shown in Figure 5.

In Figure 5, the tool system employs a hard alloy boring tool with machine clip. The tool angles are as follows: rake angle of 5°, relief angle of 8°, end relief angle of 10°, tool cutting edge angle of 45°, tool minor cutting edge angle of 3°, and inclination angle of 0°. The workpiece bore diameter is 50 mm and the drill length is 3 m. The cutting speed of the tool during the machining process is 10 meters per minute, with a depth of cut of 0.1 millimeters and a feed rate of 0.1 millimeters per revolution.

Table 1: Values of variable parameters.

Parameters	First	Second	Third
h	0.25	1/3	0.5
V_0	5 m/s	10 m/s	15 m/s

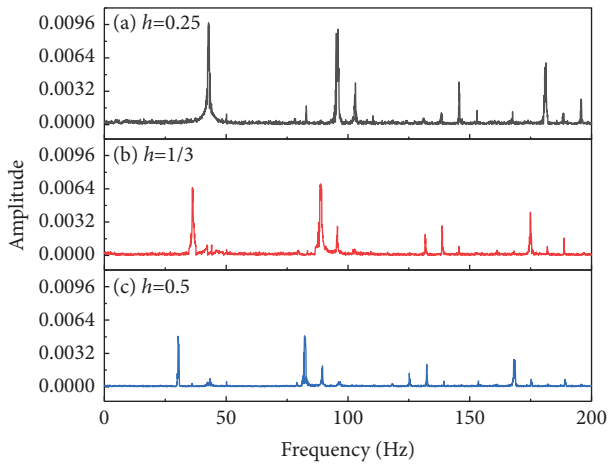

Figure 6: Power spectrum of transverse vibration amplitude under different liquid filling ratio.

3.1.2. Experimental Scheme. First, set the environment parameters of the system to be the same as those of the numerical simulation, and then collect the single variable signal with the filling ratio (h) and cutting fluid flow velocity (V_0) as the variables, respectively. Finally, determine the influence of each parameter change on the system stability through power spectrum analysis. The selection of variable parameters is shown in Table 1.

3.2. Experimental Data Analysis. In this paper, the influence of parameter changes on the stability of the system is studied through the power spectrum characteristics of the transverse vibration amplitude. The full name of the power spectrum is the power spectrum density function, which is defined as the signal power in the unit frequency band. It can transform the vibration description in the time domain into the vibration description in the frequency domain, so it can be used as an effective tool for the analysis of system vibration characteristics [44, 45].

According to data analysis, when the liquid-filled ratio h changes, the power spectrum of transverse vibration amplitude is shown in Figure 6:

It can be seen from the power spectra in Figure 6 that with the increase of the liquid filling ratio h, although the frequencies of each order of resonance in the system remain unchanged, the spectral peaks of each order of frequency gradually decrease. This indicates that the vibration characteristics of the system are weakened and the stability of the system is enhanced with the increase of liquid filling ratio h. This is consistent with the effect of liquid-filled ratio h change on system stability in Figures 2 and 3.

When cutting fluid velocity changes V_0, the power spectrum of transverse vibration amplitude is shown in Figure 7.

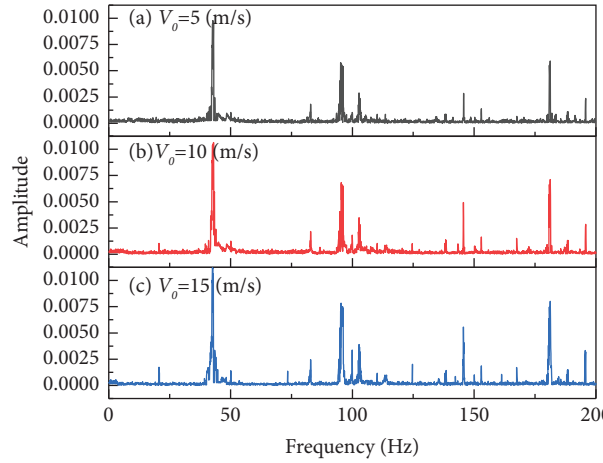

Figure 7: Power spectrum of transverse vibration amplitude at different cutting fluid flow velocities.

From Figure 7, with the increase of the cutting fluid flow velocity, although the resonance point of the system is unchanged, the system's discrete spectrum peak gradually increased, and the peak value is getting larger. This shows that the increase of the cutting fluid velocity aggravates the chaotic characteristics of the system, which is consistent with the numerical simulation results in Figures 2(b) and 2(c).

4. Conclusion

In this paper, the nonlinear lateral vibration motion equation of the BTA deep-hole machining system is established by analyzing the internal cutting fluid effect. On this basis, the chaotic characteristics of the system are studied systematically; and by combining numerical simulation and physical experiment, the mechanism of the dynamic stability of the system under the changes of filling ratio, cutting fluid flow velocity, and frequency ratio was preliminarily obtained.

(1) In precision boring, the increase of the liquid filling ratio improves the system quality, reduces the system frequency, and causes the resonance frequency of the system to decrease, which reduces the resonance area and weakens the chaotic characteristics of the system. Therefore, in the actual machining process, increasing the filling ratio is one of the measures to improve the stability of the machining system.

(2) In precision boring, the increase of cutting fluid velocity will change the movement of fluid and aggravate the chaotic effect of the system. Therefore, under the condition of meeting the production demand, the cutting fluid velocity should be reduced as much as possible to improve the stability of the system.

(3) When the frequency ratio changes in a small range, the frequency doubling relationship between the disturbance frequency and the system frequency is

not easy to trigger, the probability of resonance of the system is reduced, and the system stability is good. When the frequency ratio changes in a large numerical range, the frequency doubling relationship between the disturbance frequency and the system frequency is easy to trigger, which increases the probability of resonance of the system, and the system stability is poor. Therefore, in the actual processing process, the resonance region can be avoided by adjusting the frequency ratio value range to improve the stability of the system.

In summary, the research conclusions of this paper on the dynamic stability of the BTA deep-hole machining system under the consideration of the internal cutting fluid effect can lay a certain theoretical foundation for the analysis, control, and optimization of its complex mechanical behavior in engineering practice.

Data Availability

The data used to support the findings of this study are included within the article.

Conflicts of Interest

The authors declare that they have no conflicts of interest.

Acknowledgments

This work was supported by the National Natural Science Foundation of China (no. 51075126) and Scientific and Technological Research Project of Henan Provincial Science and Technology Department (no. 192102210052).

References

[1] A. Luongo, M. J. Leamy, S. Lenci, G. Piccardo, and C. Touze, "Advances in stability, bifurcations and nonlinear vibrations in mechanical systems," *Nonlinear Dynamics*, vol. 103, no. 4, pp. 2993–2995, 2021.

[2] C. H. Miwadinou, A. V. Monwanou, L. A. Hinvi, V. K. Tamba, A. A. Koukpémèdji, and J. B. Chabi Orou, "Nonlinear oscillations of nonlinear damping gyros: resonances, hysteresis and multistability," *International Journal of Bifurcation and Chaos*, vol. 30, no. 14, Article ID 2050203, 2020.

[3] Y. V. Mikhlin and N. V. Perepelkin, "Non-linear normal modes and their applications in mechanical systems," vol. 225, no. 10, pp. 2369–2384, 2011.

[4] D. Biermann, F. Bleicher, U. Heisel, F. Klocke, H. C. Möhring, and A. Shih, "Deep hole drilling," *CIRP Annals*, vol. 67, no. 2, pp. 673–694, 2018.

[5] J. B. Chandar, L. Nagarajan, and M. S. Kumar, "Recent research progress in deep hole drilling process: a review," *Surface Review and Letters*, vol. 28, no. 11, Article ID 2130003, 2021.

[6] H. M. Al-Wedyan, R. B. Bhat, and K. Demirli, "Whirling vibrations in boring trepanning association deep hole boring process: analytical and experimental investigations," *Journal of Manufacturing Science and Engineering*, vol. 129, no. 1, pp. 48–62, 2007.

[7] H. Al-Wedyan, *Control of Whirling Vibrations in BTA Deep Hole boring Process Using Fuzzy Logic Modeling and Active Suppression Technique*, Concordia University, Montreal, Canada, 2004.

[8] S. Wang, *Deep Hole Processing Technology*, Northwestern Polytechnic University Press, Xi'an, China, 2003.

[9] W. Zhao, B. Huo, and D. Huang, "Nonlinear transverse vibration induced by fluid disturbance on BTA deep hole precision reaming system," *Journal of Mechanical Engineering*, vol. 56, no. 17, pp. 155–164, 2020.

[10] H. M. A. Wedyan and M. T. Hayajneh, "Dynamic modelling and analysis of whirling motion in BTA deep hole boring process," *International Journal of Machining and Machinability of Materials*, vol. 10, no. 1/2, pp. 48–70, 2011.

[11] G. Ma and X. Shen, "Eigensolution of a BTA deep-hole drilling shaft system," *Journal of Mechanical Science and Technology*, vol. 32, no. 4, pp. 1499–1504, 2018.

[12] K. Weinert, O. Webber, and C. Peters, "On the influence of drilling depth dependent modal damping on chatter vibration in BTA deep hole drilling," *CIRP annals*, vol. 54, no. 1, pp. 363–366, 2005.

[13] M. S. Khan and M. I. Khan, "A novel numerical algorithm based on Galerkin–Petrov time-discretization method for solving chaotic nonlinear dynamical systems," *Nonlinear Dynamics*, vol. 91, no. 3, pp. 1555–1569, 2018.

[14] H. Arvin, A. Arena, and W. Lacarbonara, "Nonlinear vibration analysis of rotating beams undergoing parametric instability: lagging-axial motion," *Mechanical Systems and Signal Processing*, vol. 144, Article ID 106892, 2020.

[15] W. Jia, F. Gao, Y. Li, W. Wu, and Z. Li, "Nonlinear dynamic analysis and chaos prediction of grinding motorized spindle system," *Shock and Vibration*, vol. 201910 pages, Article ID 9643124, 2019.

[16] B. Ma and Y. Ren, "Nonlinear dynamic analysis of the cutting process of a nonextensible composite boring bar," *Shock and Vibration*, vol. 202013 pages, Article ID 5971540, 2020.

[17] J. H. Chin, C. T. Hsieh, and L. W. Lee, "The shaft behavior of BTA deep hole drilling tool," *International Journal of Mechanical Sciences*, vol. 38, no. 5, pp. 461–482, 1996.

[18] Y. L. Perng and J. H. Chin, "Theoretical and experimental investigations on the spinning BTA deep-hole drill shafts containing fluids and subject to axial forces," *International Journal of Mechanical Sciences*, vol. 41, no. 11, pp. 1301–1322, 1999.

[19] C. S. Deng and J. H. Chin, "Roundness errors in BTA drilling and a model of waviness and lobing caused by resonant forced vibrations of its long drill shaft," *Journal of Manufacturing Science and Engineering*, vol. 126, no. 3, pp. 524–534, 2004.

[20] K. Matsuzaki, T. Ryu, A. Sueoka, and K. Tsukamoto, "Theoretical and experimental study on rifling markgenerating phenomena in BTA deep hole drilling process," *Advances in Mechanical Engineering*, vol. 88, pp. 196–205, 2015.

[21] K. Matsuzaki, A. Sueoka, T. Ryu, H. Morita, and K. Omura, "A countermeasure against a rifling mark generating phenomenon on BTA deep hole drilling process (mechanical systems)," *Transactions of the Japan Society of Mechanical Engineers. Series C*, vol. 76, no. 767, pp. 1684–1691, 2010.

[22] N. Raabe, D. Enk, D. Biermann, and C. Weihs, "Dynamic disturbances in BTA deep-hole drilling: modelling chatter and spiralling as regenerative effects," in *Advances in Data Analysis, Data Handling and Business Intelligence, Studies in Classification, Data Analysis, and Knowledge Organization*, A. Fink, B. Lausen, W. Seidel, and A. Ultsch, Eds., pp. 745–754, Springer, Berlin, Germany, 2009.

[23] N. Raabe, O. Webber, W. Theis, and C. Weihs, "Spiralling in BTA deep-hole drilling: models of varying frequencies," in *From Data and Information Analysis to Knowledge Engineering, Studies in Classification, Data Analysis, and Knowledge Organization*, M. Spiliopoulou, R. Kruse, C. Borgelt, A. Nürnberger, and W. Gaul, Eds., pp. 510–517, Springer, Berlin, Heidelberg, 2006.

[24] A. Messaoud and C. Weihs, "Monitoring a deep hole drilling process by nonlinear time series modeling," *Journal of Sound and Vibration*, vol. 321, no. 3-5, pp. 620–630, 2009.

[25] A. Messaoud, C. Weihs, and F. Hering, "Nonlinear time series modelling: monitoring a drilling process," in *From Data and Information Analysis to Knowledge Engineering*, , pp. 302–309, Springer, 2006.

[26] A. Messaoud, W. Theis, F. Hering, and C. Weihs, "Monitoring a drilling process using residual control charts," *Quality Engineering*, vol. 21, no. 1, pp. 1–9, 2008.

[27] A. Steininger and F. Bleicher, "In-process monitoring and analysis of dynamic disturbances in boring and trepanning association (BTA) deep drilling," *Journal of Machine Engineering*, vol. 18, no. 4, pp. 47–59, 2018.

[28] Z. Zhao and L. Miao, "Research on vortex motion of BTA drilling shaft caused by hydro-force," *Journal of Mechanical Engineering*, vol. 41, no. 1, pp. 230–233, 2005.

[29] M. Utsumi, "Vibration analysis of a cylindrical rotor partially filled with liquid considering nonlinearity of liquid motion," *Mechanical Engineering Journal*, vol. 7, no. 4, Article ID 19-00554, 2020.

[30] G. Wang, H. Yuan, and H. Sun, "An investigation on the instability of a flexible liquid-filled rotor," *Part G: Journal of Aerospace Engineering*, vol. 234, no. 2, pp. 165–172, 2020.

[31] B. Li, G. Wang, and H. Yuan, "An analytical investigation on the dynamic stability of a rotor filled with liquid," *Journal of Vibroengineering*, vol. 20, no. 6, pp. 2253–2267, 2018.

[32] R. D. Firouz-Abadi and M. R. Permoon, "Effect of liquid viscosity on instability of high-spinning partially-filled shell rotors," *International Journal of Structural Stability and Dynamics*, vol. 13, no. 6, Article ID 1350025, 2019.

[33] R. D. Firouz Abadi and H. Haddadpour, "The flexural instability of spinning flexible cylinder partially filled with viscous liquid," *Journal of Applied Mechanics*, vol. 77, no. 1, Article ID 011001, 2010.

[34] R. D. Firouz-Abadi, M. R. Permoon, and H. Haddadpour, "On the instability of spinning cylindrical shells partially filled with liquid," *International Journal of Structural Stability and Dynamics*, vol. 12, no. 3, Article ID 1250018, 2012.

[35] W. Zhao, Q. Zhang, W. Jia, and Z. Q. Hu, "Influence on BTA boring bar transverse vibration considering inner cutting fluid velocity and axial force," *Advanced Materials Research*, vol. 887-888, pp. 1215–1218, 2014.

[36] W. Zhao, D. Chen, and Z. Hu, "Center track analysis and simulation considering effect of vortex and perturbation of cutting fluid on BTA boring bar," *Applied Mechanics and Materials*, vol. 526, pp. 150–154, 2014.

[37] W. Zhao, B. Huo, D. Huang, and J. Zhao, "Effect of the perturbation in cutting fluid on the transverse vibration frequency in BTA deep-hole boring bar system," *Journal of Vibration and Shock*, vol. 39, no. 11, pp. 184–192, 2020.

[38] G. I. Taylor, "Stability of a viscous liquid contained between two rotating cylinders," *Philosophical Transactions of the Royal Society of London*, vol. 223, no. 605-615, pp. 289–343, 1923.

[39] H. Dou, "Stability of taylor-Couette flow between concentric rotating cylinders," in *Origin of Turbulence*, , pp. 271–304, Springer, 2022.

[40] M. Golubitsky and I. Stewart, "Symmetry and stability in Taylor-Couette flow," *SIAM Journal on Mathematical Analysis*, vol. 17, no. 2, pp. 249–288, 1986.

[41] F. Rosso, "On the pointwise stability of a viscous liquid between rotating coaxial cylinders," *Journal of Mathematical Analysis and Applications*, vol. 98, no. 1, pp. 251–269, 1984.

[42] S. T. Wereley and R. M. Lueptow, "Velocity field for Taylor–Couette flow with an axial flow," *Physics of Fluids*, vol. 11, no. 12, pp. 3637–3649, 1999.

[43] J. Guckenheimer and P. Holmes, *Nonlinear Oscillations, Dynamical Systems, and Bifurcations of Vector fields*, Springer-Verlag, New York, NY, USA, 1983.

[44] C. Jiang, Z. Zhang, and C. Li, "Vibration measurement based on multiple self-mixing interferometry," *Optics Communications*, vol. 367, pp. 227–233, 2016.

[45] M. Decker, "Vibration fatigue analysis using response spectra," *International Journal of Fatigue*, vol. 148, Article ID 106192, 2021.